Linkage mapping of root shape traits in two carrot populations

Andrey Vega, Scott H. Brainard, Irwin L. Goldman

Department of Plant and Agroecosystem Sciences, University of Wisconsin-Madison, Madison, Wisconsin, 53706, United States of America.

Corresponding Author: ilgoldma@wisc.edu, vegaalfaro@wisc.edu

Mailing address for all authors:

1575 Linden Drive, Madison, WI. 53706 USA.

Keywords: Genetic mapping, *Daucus carota* var *sativus, OFP-TRM and IQD* plant regulon.

Abstract

This study investigated the genetic basis of carrot root shape traits using composite interval mapping in two biparental populations (n=119 and n=128). The roots of carrot $F_{2:3}$ progenies were grown over two years and analyzed using a digital imaging pipeline to extract root phenotypes that compose market class. Broad-sense heritability on an entry-mean basis ranged from 0.46 to 0.80 for root traits. Reproducible quantitative trait loci (QTL) were identified on chromosomes 2 and 6 on both populations. Colocalization of QTLs for phenotypically correlated root traits was also observed and coincided with previously identified QTLs in published association and linkage mapping studies. Individual QTLs explained between 14 to 27% of total phenotypic variance across traits, while four QTLs for length-to-width ratio collectively accounted for up to 73% of variation. Predicted genes associated with the *OFP-TRM* (OVATE Family Proteins - TONNEAU1 Recruiting Motif) and *IQD* (IQ67 domain) pathway were identified within QTL support intervals. This observation raises the possibility of extending the current regulon model of fruit shape to include carrot storage roots. Nevertheless, the precise molecular mechanisms through which this pathway operates in roots characterized by secondary growth originating from cambium layers remain unknown.

Introduction

Carrot (*Daucus carota* var. *sativus, 2n=2x=18*) is a biennial vegetable crop known for its diverse root shapes (Rubatzky et al. 1999; Simon, 2021). The total national carrot production in the U.S was valued at $1.2 billion USD (about $4 per person in the U.S) in 2022 (United States Department of Agriculture - National Agricultural Statistics Service [USDA-NASS 2023]). Carrots are commercialized in market classes which are primarily determined by root shape and end-use. A carrot market class is defined as a group of carrot cultivars that share a similar root shape phenotypes and are grouped together to facilitate crop breeding and trade. In Europe, the classification of carrots by shape traces back to at least the 1600s (Banga, 1957; 1963a; 1963b)

and in In North America, by the 1940s, the USDA had already established the practice of categorizing carrot cultivars into market classes using descriptions of standard root shapes (Magruder et al. 1940).

While there are 10-15 recognized carrot market classes (Geoffriau and Simon 2020), over 80% of released carrot cultivars in the last 85 years have been classified into only four market classes, Imperator, Nantes, Chantenay and Danvers, according to *HortScience* Vegetable Cultivar Descriptions for North America (Mou et al. 2022). This emphasizes the role of market classes in carrot breeding and economics and the prevalence of certain shape types that are tied to a specific end-use. Imperator, for example, is the most used market class for baby-cut carrots in North America (Lucier and Lin 2007; Goldman 2019). Root shape traits including length, width, and curvature of the shoulders and tip play a crucial role in categorizing carrot cultivars into market classes. While traditionally assessed subjectively, these traits are now analyzed using digital imaging pipelines (Turner et al. 2018; Brainard et al. 2021, Vega and Goldman, 2023). Understanding the genetic basis of root traits composing market class is essential for carrot improvement efforts. This is because carrot breeding often occurs within market classes as inter-class crosses require lengthy breeding cycles to regain a desired shape adding to challenge of selecting for the targeted traits. Alternatively, choosing to breed using only plants within a market class to circumvent this problem may limit the availability of germplasm that is otherwise available through inter-class breeding.

Over the course of domestication, selective breeding played a role in shaping the array of root shapes observed in the collection of carrot varieties (Geoffriau and Simon 2020; Ellison 2019; Wu et al. 2018). The ability to form a storage root was key in the transition from the wild (*D. carota* var *carota)* to the cultivated carrot (*D. carota* var. *sativus*). The literature on genetic control of carrot root traits suggests two main findings: first, market class is composed of several traits and each trait is likely controlled by multiple genes (polygenic inheritance), and second,

chromosome 2 seems to be a key region associated with both the domestication syndrome and the ability of cultivated carrots to develop swollen roots.

For example, Macko-Podgórni et al. (2017) identified a polymorphism with signatures for selection on chromosome 2 which distinguished between wild and cultivated carrot accessions. The proposed gene, *DcAHLc1*, belongs to the *AT-hook* nuclear motif of plant regulatory genes, which are responsible for root tissue patterning. Similarly, using an image analysis pipeline to study root morphology, Turner et al. (2018) found evidence of colocalization of QTLs in chromosomes 1, 2 and 7 for correlated carrot root traits, suggesting these traits may be controlled by genetic linkage and quantitative inheritance. Furthermore, Brainard et al. (2022) found that phenotypic determinants of market class in carrot are under additive but highly polygenic genetic control. The authors also identified QTLs for four morphological traits that compose root market class in carrot. This included a significant SNP on chromosome 2 associated with root fill, defined as the degree to which a carrot maintains its full width along its length. Their results also indicate the presence of an *OFP8-like* transcription factor less than 40 kb of a significant QTL identified for maximum width on chromosome 3. *OFP8-like* belongs to the *OFP-TRM* (OVATE Family Protein - TONNEAU1 Recruiting Motif) and *IQD* (IQ67 domain) pathway which contain conserved domains involved in regulating biological shape by modulating patterns of cell division in plants.

The plant-specific *OFP-TRM* and *IQD* regulatory pathway is implicated in shape patterning and is well-studied in various plant organs including fruit, leaves, stems, and tubers (van der Knaap et al. 2014; Pan et al. 2017; Li et al. 2023) However, the understanding of the role that this plant shape regulon plays in true roots in carrots remains limited. To the best of our knowledge, the only study linking the *OFP-TRM* and *IQD* regulon to root shape control is in radish (*Raphanus sativus*) (Wang et al., 2020).

These pathways, conserved across plant species of economic and research importance, determine plant organ shape by regulating cell division patterns and integrating external cues

(Bürstenbinder et al. 2017; Zhao et al. 2018; Schaefer et al. 2017). Interactions within the *OFP-TRM* and *IQD* pathway also influence protein complex localization, microtubule organization, and cell division patterns which determinate plant organ shape (Lazzaro et al. 2018; Yang et al. 2020). Research suggests the involvement of the *OFP-TRM* and *IQD* pathways in phytohormone biosynthesis and signaling, microtubule reorganization, and protein interactions (van der Knaap and Østergaard, 2018; Zhang et al. 2022). The study of the plant-specific *OFP-TRM* and *IQD* regulatory pathways in carrot genetics may help explain the diversity of root shapes that current genetic models cannot entirely explain.

In this study, we conducted linkage mapping of two carrot populations to explore the genetic basis of root traits associated with market class. Our objective was to identify loci controlling root shape differences, describe the genetic basis of root shape traits, and investigate whether members of the *OFP-TRM* and *IQD* regulon overlapped with root shape QTLs. Understanding the genetic architecture of root traits can inform breeding decisions and open new opportunities for expansion beyond the carrot market classes available today.

Materials and Methods

Plant Materials

Two $F_{2:3}$ carrot (*Daucus carota* var. *sativus*) mapping populations, L1408×W133 and L1408×W279 were derived from multiple plants of male-fertile founders ‘L1408’, ‘W133’ and ‘W279’ (Figure 1A). Founder ‘L1408’ is a long Imperator type developed by the USDA Vegetable Crops Research Unit. ‘W133’ is a medium-length Danvers type, with a tapering root and acuminate tip and ‘W279’ is a bulkier wedge-shaped Chantenay type, both developed by the University of Wisconsin-Madison (Goldman, 1996). Seed of each founder was grown in the field in 2017, harvested 100-120 days after planting and vernalized for at least six weeks at 5 °C. Flowering-competent roots of each founder were planted in pots at the University of Wisconsin-

Madison Walnut St. Greenhouse and kept at 22 ± 2 °C, 42 ± 8 % relative humidity, and 16 h photoperiod. All crosses were performed starting 5-8 weeks after potting using pollination cages for isolation (Rubatzky et al. 1999) and blue bottle fly pollinators (*Calliphora vomitoria,* sourced from Forked Tree Ranch, Port Hill, Idaho).

In the L1408×W133 population, two F_1 plants (Figure S1) derived from the cross 'L1408' (♀) × 'W133' (♂) were grown in the field (2018), vernalized and self pollinated in the greenhouse to obtain F_2 progeny. Individual F_2 plants were field grown from seed the following year (2019), vernalized and self pollinated, resulting in 119 $F_{2:3}$ families. Similarly, in the L1408×W279 population two plants of each 'L1408' and 'W279' founder were cross pollinated in pairs resulting in two reciprocal crosses. Two F_1 plants were obtained from the L1408 (♀) × W279 (♂) cross and one F_1 plant from the W279 (♀) × L1408 (♂) cross (Figure S1). All three F_1 plants were grown in the field in 2018, and individually self pollinated in the greenhouse to obtain F_2 progeny as described previously. Each F_2 plant was grown in the field from seed the following year (2019). Roots were vernalized as described previously and individually self pollinated resulting in 128 distinct $F_{2:3}$ families.

The root shape in the F_1 generation of both populations displayed consistent uniformity (Figure S1), despite both mapping populations being derived from multiple founders and F_1 plants.

Field-based experimental design

All $F_{2:3}$ progenies from both populations were grown in field experiments at Jack's Pride Farms, Randolph, Wisconsin, U.S in the years 2020 and 2021. The type of soil at the experimental site is classified as a Houghton Muck (Typic Haplosaprists) with weak, medium granular structure and with an organic matter content of 20% (USDA, National Cooperative Soil Survey 2021; Colquhoun et al. 2019). This type of soil is commonly used in commercial carrot production in Wisconsin. All experiments were planted in a randomized complete block design

with one genotype replication per block in each of two blocks. Experimental units of 1-m rows were randomized within each block. Carrot seed was hand planted in raised beds 1.8-m-wide (center to center) and 0.40-m-high at 5 cm spacing between plants and 37.5 cm between rows. Experiments were planted on April 26, 2020, and May 10, 2021, and harvested August 19, 2020, and August 24, 2021. A subsample of 10, or all if less than 10 roots were available, were harvested from the center of the row and stored at 5˚C until phenotyping.

Phenotyping

Phenotyping was conducted following the digital imaging procedure established by Brainard et al. (2021). The phenotyping process is delineated and visualized in Figure S2. Every $F_{2:3}$ family within each of two mapping populations was cultivated in the years 2020 and 2021. Each $F_{2:3}$ family had one experimental row, replicated in two blocks each year. We sampled 10 roots per row, or all available if less than 10. In total, the number of roots phenotyped amounted to 8,841.

All measured traits were estimated from root straight masks derived from digital images (Figure S2). Root length (mm) was defined as the distance between the center of the root crown and the root tip. Maximum width (mm) was measured as the widest diameter along the root and was only used to estimate length-to-width ratio. Width (mm) was defined as the diameter of the root at the 50-th percentile of its length (mm). Length-to-width ratio was calculated as the ratio of root length to maximum width. Biomass was estimated as the two-dimensional area of the straight mask (mm^2), also referred to as digital biomass in the digital phenotyping literature. Two additional traits, namely shoulder curvature and tip curvature, were derived by performing Principal Component Analysis (PCA) on contour values at the first 50 pixels and last 50 pixels of each root's straight mask respectively (Brainard et al. 2021). To capture size-independent variation in the PCA-derived traits, straight masks were normalized to a width of 1 and a length of 1000. To visualize the phenotypic variables of length-to-width ratio, shoulder curvature, and

tip curvature, Figure S3 presents roots at the 1st and 99th percentiles of their respective distributions. This illustration is informative given that length-to-width ratio is a proportion of two linear measurements (length and maximum width), while shoulder and tip curvature derive from principal component scores.

Genotyping

To infer $F_{2:3}$ genotypes, ~10 $F_{2:3}$ seeds were planted in conical tubes filled with Pro-Mix High Porosity media (Premier Tech, Quakertown, PA) at the University of Wisconsin-Madison Walnut St. Greenhouses in December of 2021. Plants were maintained at 22 ± 2 °C and 42 ± 8 relative humidity with a 16 h photoperiod. At 4 to 5 weeks after planting, 1 cm^2 of leaf tissue was sampled for each of the ~10 plants per $F_{2:3}$ family and bulked. Heterozygous genotypes in the F_2 generation are expected to segregate in a 1:2:1 ratio after one round of inbreeding ($F_{2:3}$ generation). Because only two founders are present in each biparental population, the expected allele frequency for heterozygote genotypes in the $F_{2:3}$ generation is 1:1, which allows for accurate identification of heterozygous $F_{2:3}$ genotypes given sufficient read depth. Leaf tissue was stored at -80 °C for at least 72 h and lyophilized. Lyophilized tissue was macerated, mixed, and 10-50 mg of each bulk sample was transferred to Collection Microtube plates (Giagen, Germantown, MD). P

lates were submitted for DNA extraction and Genotyping by Sequencing (GBS) to the University of Wisconsin-Madison Biotechnology Center. Genomic DNA extraction was completed using the QIAGEN DNeasy mericon 96 HT kit and the automated extraction robot QIACube HT (Qiagen, germantown, MD). Quantification of DNA was performed using the Quant-iT™ PicoGreen dsDNA kit (Life Technologies, Grand Islan, NY). GBS libraries were prepared following Elshire et al. (2011). Restriction enzyme *ApeKI* was used to digest DNA followed by annealing of sample-specific barcodes and Illumina adapters. Multiplexed samples were sequenced using an Illumina NovaSeq 6000 sequencer. On average, 8.5 million reads

were obtained per sample. Discovery of single nucleotide polymorphisms (SNPs) was performed by the Bioinformatics Resource Core (https://bioinformatics.biotech.wisc.edu/) using Tassel GBS Version 2 (Glaubitz et al. 2014) and version 3 of the carrot reference genome (Coe et al. 2023). In populations L1408×W133 and L1408×W279, approximately 280,000 unfiltered variants were detected. Initial marker filtering was performed using bcftools (Li, 2011). Insertion deletion markers (indels) were removed and only bi-allelic SNPs with a 95th percentile of read depths and genotype quality scores ≥ 20 and minor allele frequencies > 0.05 were retained, resulting in 15,078 and 7,275 markers for populations L1408×W133 and L1408×W279 respectively.

Linkage map construction

Additional marker filtering and linkage map construction were performed for each population individually using custom R scripts (R Core Team, 2022) and the R package MapRtools (v. 0.30; Endelman 2023). R code and data are available in the Zenodo repository (10.5281/zenodo.10023295). Because a high proportion of heterozygous SNP markers were identified and coincided with highly repetitive regions, markers and $F_{2:3}$ individuals with heterozygote genotype frequencies outside the range of 0.10-0.90 and ≥ 10% missing data were removed. Population L1408×W279, was derived from two plants of each founder ('L1408' and 'W279'). Both founder genotypes showed unexpected high genetic heterogeneity (Table S1). As a result, only markers shared by all L1408×W279 founders were kept, leading to a reduced number of markers available for constructing the L1408×W279 linkage map.

Markers for all progeny in each population were recoded (phased) according to the founder genotypes for each population. The 'L1408' allele was designated as the reference 'A' allele, while the alternative 'B' allele originated from either the founder 'W133' or 'W279' accordingly. 'A' and 'B' denote the two homozygous states and 'H' the heterozygote. In the founders, only homozygous markers (A×B and B×A types; Braun et al. 2017) were retained for

initial genetic map construction resulting in 4,734 and 543 markers for populations L1408×W133 and L1408×W279 respectively. Additional filtering and marker binning at a threshold of r^2= 0.99 using the LDbin function from MapRtools resulted in 2,367 and 361 marker bins for populations L1408×W133 and L1408×W279 respectively. Nine linkage groups corresponding to the nine carrot chromosomes were formed at a logarithm of odds (LOD) threshold of 17 for L1408×W133 and 25 for L1408×W279. Linkage groups were each trimmed individually and for each population using MapRtools functions LG and plot_genofreq. Resulting markers after linkage group trimming were ordered according to version 3 of the carrot reference genome (Coe et al. 2023). Map distances were estimated using the Kosambi mapping function (Kosambi, 1943) and 19-point multiple regression using the function genetic_map. Composite interval mapping (CIM) was conducted using Haley-Knott regression, a 10 cM window size, and one to three marker covariates under a single QTL model using the R/qtl cim function. A 1.5-LOD support interval was estimated for identified QTLs using the functions stepwise and lodint (Broman, 2023). Genome-wide linkage disequilibrium (LD) decay was estimated and plotted using the MapRTools function plot_LD. Only markers with homozygous states in the founders (A×B and B×A types) were used to construct the genetic maps. However, to fill gaps in the linkage map for chromosomes 3, 8, and 9 of the L1408×W279 population, we incorporated an additional 18 heterozygous markers (Table S2).

Statistical analysis

Phenotypic data were analyzed using custom R scripts and the function lmer from the R package lme4 (Bates et al. 2015) in a two-stage analysis approach (Piepho et al 2012). In Stage 1, each genotype was represented by the Best Linear Unbiased Estimate (BLUE) computed across years using the following model:

$$Y_{ijk} = g_i + y_j + b_{k(j)} + gy_{ij} + \varepsilon_{ijk}$$

Where, Y_{ijk} represents the phenotypic response associated with root shape, g_i is the *i*-th genotype, y_j is the *j*-th year, $b_{k(j)}$ is the *k*-th block nested within the *j*-th year, gy_{ij} is the interaction of the *i*-th genotype and the *j*-th year and ε_{ijk} are the residuals, with $\varepsilon_{ijk} \sim iid, N(0, \sigma_\varepsilon^2)$. The same model with all terms fit as random effects, was used to estimate broad-sense heritability (H^2) on an entry-mean basis from Stage 1 variance components:

$$H^2 = \frac{\sigma_G^2}{\sigma_G^2 + PEV} \quad (1)$$

In equation 1, σ_G^2 is the variance associated with genotypes and *PEV* is the prediction error variance. *PEV* is given by:

$$PEV = \frac{\sigma_{Gy}^2}{y} + \frac{\sigma_\varepsilon^2}{ry} \quad (2)$$

In equation 2, σ_{Gy}^2 is the variance component associated with genotype by year interactions, σ_ε^2 is the residual variance, y is the number of years ($y = 2$) and r is the number of replicates ($r = 2$). The Stage 1 BLUEs were used as the response variable for linkage mapping in Stage 2. Each phenotypic trait was fit independently. Across experiments, any phenotypic BLUE outside 3 times the standard deviation above or below the mean was removed as an outlier. Multiple means comparison between the founder phenotypes and effects of allele substitution were performed using the functions emmeans and cld from the emmeans and multicomp R packages (Hothorn et al. 2008; Lenth, 2020).

Candidate genes

Candidate genes in the QTL intervals were identified using BLAST search. To address challenges associated with slow LD decay and large LD blocks impacting QTL size estimation, we targeted homolog genes in the *OFP-TRM* and *IQD* regulon, recognized for their role in shaping plant organs (Li et al. 2023). Amino acid sequences of 34 *IQDs*, 27 *OFPs*, and 26 *TRMs* genes involved in the control of fruit shape in tomato (*Solanum lycopersicum*) were obtained from the Solgenomics database (https://solgenomics.net/locus). To identify homologs

of *IQDs*, *OFPs*, and *TRMs* in carrot, a protein BLAST search was conducted using the NCBI database. Carrot candidate gene information was obtained from the NCBI gene database (https://www.ncbi.nlm.nih.gov/gene). To better characterize predicted genes and infer homology between specific sequences in chromosomal regions encompassing QTL intervals, multiple sequence alignment was performed using Clustal Omega (https://wwwdev.ebi.ac.uk/Tools/jdispatcher/msa). This alignment included known regulators of shape from tomato and carrot candidate genes within a 2 Mb interval of QTL peaks. Motif alignment was conducted using MAST (Timothy et al. 1998) from the MEME suite (https://meme-suite.org/meme/doc/mast.html) to describe four previously uncharacterized predicted carrot genes, DCAR_027681, DCAR_017186, DCAR_21448, and DCAR_008585 (File S1). Amino acid sequences of carrot and tomato *IQDs*, *OFPs*, and *TRMs* are available (File S2).

Results

Phenotypic description

To generate two carrot populations segregating for root shape, the long Imperator type 'L1408' was crossed with the bulkier Danvers type 'W133' and the Chantenay type 'W279'. Root shape trait distributions in both populations showed that the founders were primarily located at the distribution extremes (Figure S4 and Figure S5). Significant differences among all founders were observed in root width, shoulder and tip curvature as well as length. However, no significant differences were found between ‘W133’ and ‘W279’ in length-to-width ratio and biomass (Figure 1). Generally, 'L1408' and 'W279' exhibited pronounced phenotypic differences, while 'W133' showed intermediate phenotypes across all measured traits, except for length.

The root shape in the F_1 generation of both populations displayed phenotypic uniformity (Figure S1). This supports our assumption that QTLs for shape traits in these populations carries just two alleles per loci, one from each founder, despite both mapping populations were

derived from multiple founders and F_1 plants, and unexpected genetic heterogeneity was observed for all founders (Figure S1 and Table S1).

Phenotypic correlations

Root length and length-to-width ratio showed positive correlations, ranging from 0.73 to 0.82, while width showed a negative correlation of -0.64 with length-to-width ratio across populations (Figure 2). Consistent with previous studies, positive correlations were found between length and biomass (Vega and Goldman, 2023; Figure 2). No significant correlations were observed between length and width, as well as between biomass and length-to-width ratio. Biomass has been identified as a trait related to root size, while length-to-width ratio has been associated with root shape. Moreover, no significant correlations were detected between biomass and either shoulder curvature or tip curvature (Figure 2).

Variance partitioning and heritability

The broad-sense heritability on an entry-mean basis was 0.70 for width and 0.80 for length-to-width ratio, indicating high precision in the measurement of these traits for both mapping populations (Table 1). For shoulder curvature, tip curvature, biomass, and length the broad-sense heritability ranged from 0.46 to 0.75 across years and populations (Table 1). These heritability estimates align with previous studies that have reported similar estimates for length-to-width ratio and length, which are traits related to root shape and comprise market class in carrots (Turner et al. 2018; Brainard et al. 2021).

Phenotypic data across years were combined for QTL mapping as the genotype variance exceeded the genotype × year interaction by a factor of three for all traits, except for tip curvature where the ratio was approximately 1.5 (Table 1). Tip curvature is a trait influenced by environmental factors (Vega and Goldman 2023) and with moderate to low estimates of heritability (Table 1; Brainard et al. 2021).

Linkage map quality

Hierarchical clustering confirmed that each mapping population behaved as a single $F_{2:3}$ population (Figure S6), despite both mapping populations were derived from multiple founders and F_1 plants, and unexpected genetic heterogeneity was observed in all founders (Table S1).

A separate linkage map was constructed for each mapping population, using 2,150 GBS-derived SNP markers for L1408×W133 and 341 markers for L1408×W279. (Table 2). The length of the linkage map was 690 cM for L1408×W133 and 406 cM for L1408×W279. Both map lengths fell within the range of carrot mapping populations (Ellison et al. 2017; Turner et al. 2018; Bannoud et al. 2019, Coe et al., 2023). Markers were ordered according to the physical position of version 3 of the carrot genome (Figure S7 and Figure S8). Linkage map resolution ranged from 0.3 to 1.2 markers/cM across populations (Table 2), consistent with the linkage maps reported by Parsons et al. (2015) and Bannoud et al. (2019).

The maximum marker spacing was 22.5 cM on chromosome 8 for the L1408×W279 population. Genetic heterogeneity in the founders (Table S1) resulted in reduced marker coverage on the proximal arms of chromosomes 2, 4, and 6 in both populations, as well as on chromosomes 7 and 8 in populations L1408×W133 and L1408×W279, respectively (Figure S7 and Figure S8). This reduced coverage was attributed to a higher proportion of heterozygous to homozygous markers in the centromeres and at the proximal and distal ends of the chromosomes in both populations (Figure S9 and Figure S10). Heterozygosity hotspots in our populations closely coincided with the reported positions of chromosomal centromeres and repetitive regions according to the telomere-to-telomere carrot genome assembly (Figure S9-S10; Wang et al. 2023). An explanation for the observed high heterozygosity is that instead of these regions being heterozygous variations in the DNA sequence (e.g., each founder contributing a different allele at this locus), these heterozygous SNPs could be artifacts that resulted from the mapping of reads of a given repetitive DNA sequence. In this scenario, the two copies of repetitive DNA may only differ by a single SNP and during read alignment, the

software might interpret them as heterozygous SNP calls across the entire mapping population when they aren't truly heterozygotes. True heterozygous calls are not expected at high frequency on an $F_{2:3}$ mapping population, thus we filtered for heterozygote marker frequencies outside the range of 0.1 < or > 0.90 to avoid this issue. In addition, heterozygous markers in the founders were excluded from the initial map construction, but 18 heterozygous markers were added to the linkage map of the L1408×W279 population to improve coverage in chromosomes 3, 8 and 9 (Table S2). The higher proportion of heterozygous to homozygous markers in the centromeres and chromosome ends of both populations may be characteristic of the outcrossing mating system of carrots which maintain high levels of heterozygosity due to severe inbreeding depression (Rong et al. 2010, Glémin et al. 2006; Iorizzo et al. 2013; Iorizzo et al. 2016).

As expected, genome-wide LD was slow decaying for both populations. In population L1408×W133, a value of $r^2 = 0.15$ intersected physical distance at 28 Mb and genetic distance at 58 cM. In population L1408×W279, a value of $r^2 = 0.15$ intersected physical distance at 26 Mb and genetic distance at 29 cM (Figure S11).

QTL analysis of root shape traits in two carrot mapping populations

Significant QTL regions associated with root shape traits were identified on chromosomes 2, 3, 5, 6, and 8 in the L1408×W133 population (Figure 3A, Table S3). Chromosomes 2 and 5 contained single QTLs for length-to-width ratio, and shoulder curvature, respectively (Figure 2A). Chromosomes 3, 6, and 8 harbored QTLs for width, length-to-width ratio, and tip curvature (Figure 3, Table S3). These QTLs on chromosomes 3, 6 and 8 colocalized because of strong phenotypic correlations (Figure 2).

The 1.5 LOD support interval for QTLs on chromosomes 2, 5, 6, and 8 encompassed four previously uncharacterized carrot genes: DCAR_027681, DCAR_017186, DCAR_21448, and DCAR_008585 (Table S4). These uncharacterized genes were identified as *TRM* homologs

through BLAST searches and motif alignment (File S1). Further, three of these four predicted carrot genes exhibited the M8 motif, while the fourth gene had the M2 motif (File S1). Both M8 and M2 motifs have been described by Wu et al. (2018) as conserved *TRM* motifs. Multiple sequence alignment revealed relationships between *TRM* homologs in carrot and tomato (Figure S12). To simplify nomenclature, the uncharacterized carrot genes were renamed after their related tomato homologs (Figure S12) and annotated as such in Figure 3.

Reproducible QTLs

Reproducible QTLs for width on chromosome 6 and for length-to-width ratio on chromosome 2 were identified in both populations (Figure 4). The 1.5-LOD support intervals overlapped across the two mapping populations, confirming the reproducibility of QTLs for length-to-width ratio on chromosome 2 and width on chromosome 6. (Figure 4 and Table S3). These two QTLs explained 16 to 17% of width and 14 to 20% of the length-to-width ratio phenotypic variation across both mapping populations (Table S3).

In the L1408×W133 population, individuals that inherited either one or two copies of the 'W133' (B) allele at the QTL for width on chromosome 6 resulted in a width increase of 3.0 mm or 1.0 standard deviation units (Figure 5A). No significant difference in width was detected between individuals that inherited either one or two copies of the ‘W133’ allele (Figure 5A), and the dominance degree was 0.7 (Table S3). These two findings suggest partial dominance to the ‘W133’ phenotype in width (Table S3, Figure 5A).

In the L1408×W279 population, individuals carrying two copies of the 'W279' (B) allele at the root with QTL on chromosome 6 showed an increase of about 3.2 mm or 1.2 standard deviation units in root width while individuals inheriting a single copy of the ‘W279’ allele showed an increase of 1.8 mm or 0.73 standard deviation units (Figure 5C). Significant differences in width were detected between individuals that inherited 0, 1 or 2 copies of the ‘W279’ allele, illustrating the additive relation between the trait and the underlying QTL.

Taken together, the data suggest that inheritance of either 'W133' or 'W279' alleles at this root width QTL on chromosome 6 resulted in increased root width. In population L1408×W133, the relation was partially dominant to the W133 phenotype while in population L1408×W279 the relationship was additive (Figure 5A and C).

For the length-to-width ratio QTL on chromosome 2, two copies of the ‘W133’ allele at the QTL reduced the score by 2.0 units or approximately 1.2 standard deviation units in the L1408×W133 population (Figure 5B). No significant difference was detected between individuals that inherited either one or two copies of the ‘W133’ allele (Figure 5B). However, individuals that inherited 1 or 2 copies of the ‘W133’ allele were significantly different from those that inherited 0 copies. Similar trends were observed in the L1408×W279 population. Two copies of the ‘W279’ allele reduced the length-to-width ratio by 2.0 units or approximately 1.3 standard deviation units (Figure 5D). However, no statistical difference was found in length to width ratio in individuals that inherited either 0 or 1 copies of the alternative ‘W279’ allele.

In sum, individuals that inherited two copies of the 'W133' allele showed no statistical difference from heterozygote individuals in length-to-width ratio, indicating partial dominance to the ‘W133’ parent phenotype (Figure 5B). In contrast, in population L1408×W279 only individuals that inherited two copies of 'W279' showed significant differences in length-to-width ratio compared with individuals that inherited one or zero copies (Figure 5D), suggesting partial dominance to the ‘L1408' parent phenotype. Across both populations the effects for width and length-to-width ratio were maintained, but the gene action was population specific. Dominance degree values ranged between 0.3 and 0.7 for both traits which suggest partial dominance, and intermediate phenotypes for the heterozygote individuals (Table S3, Figure 5D).

Population Specific QTLs

In the L1408×W133 population, QTLs for length-to-width ratio were found on chromosomes 3, 6, and 8, along with an additional QTL for root width on chromosome 3. These

population-specific QTLs collectively explained an additional 53% of the phenotypic variation in length-to-width ratio and an additional 16% in root width, resulting in a total of 73% and 33% variance explained for length-to-width ratio and root width respectively (Table S3).

QTLs for tip curvature on chromosome 3 (16% variance explained), shoulder curvature on chromosome 5 (22% variance explained), and root length on chromosomes 6 and 8 (40% variance explained) were also identified (Table S3). A QTL peak for biomass explained 14% of variance and mapped to the same region of chromosome 8 (Figure 3, Table S3).

In the L1408×W279 population, one additional QTL for shoulder curvature and one QTL for length were identified in the reproducible region on chromosome 2, explaining 20% and 11% of the phenotypic variation, respectively (Figure 3, Table S3). Predicted gene members of the *TRM-OFP* and *IQD* plant organ shape regulon fell within the 1.5 LOD QTL support interval of population specific root shape QTL peaks in chromosomes 3, 5 and 8 (Figure 3, Table S4). In chromosomes 8 and 3, QTL peaks for length and length to width ratio were also colocalized suggesting tight genetic linkage and correlations among traits. In chromosome 5, however, a single QTL for shoulder curvature was identified and was in very close proximity to predicted gene members of the *TRM-OFP* and *IQD* regulon (Fig 3). All chromosomal regions harboring significant QTLs identified in the L1408×W279 population were also identified in the L1408×W133 population.

Discussion

Linkage maps

Our linkage mapping approach identified reproducible QTLs on chromosomes 2 and 6 using two independent populations, despite coverage gaps in proximal ends of several chromosomes (Figure S7 and Figure S8). Because centromeres are composed of highly repetitive and methylated sequences, the GBS *ApeKI* enzyme is less efficient and therefore large DNA fragments are produced during the reduced representation step of GBS, which are

later discarded at the read size selection step, resulting in reduced marker coverage in centromeres and telomeres (Aballay et al. 2021). In addition, unexpected genetic heterogeneity of the W279 founders contributed to a reduced linkage map in the L1408×W279 map.

A 22.5 cM gap was found in chromosome 8 of population L1408×W279. However, Turner et al. (2018) reported a linkage map with an 18 cM gap in chromosome 6, which is only a ~5 cM difference from largest gap reported here, despite Turner et al. (2018) used a larger population size (n=461) and a comparable number of markers (640). These limitations likely arise from phenomena like segregation distortion, reference genome bias, inbreeding depression, residual heterozygosity, and genetic heterogeneity in inbred lines, rather than being population specific.

QTLs associated with root shape traits composing market class

Four QTLs controlling length-to-width ratio were identified, collectively explaining 73% of the phenotypic variation (Table S3). The QTL on chromosome 2 for length-to-width ratio was reproducible (Figure 4), and QTL intervals for the same trait on chromosomes 2, 3, and 8 coincided with chromosomal regions containing predicted gene members of the *OFP-TRM* and *IQD* regulon (Fig 2, Table S3). A second reproducible region on chromosome 6 harbored a QTL for root width in both populations (Figure 4).

In the L1408×W133 population, genomic regions on chromosomes 3, 5, and 8 showed significant QTLs with 1.5 LOD intervals that encompassed carrot *OFP-TRM* and *IQD* predicted genes. However, these same regions did not exhibit such QTLs in the L1408×W279 population (Fig 3). This observation suggests variations in QTLs across different mapping populations, a concept discussed in linkage mapping literature (Holland, 2007; Myles et al., 2009). Biparental populations represent the genetic diversity existing in only two parents, which could limit the scope of identified QTLs to the studied genetic backgrounds (Michel et al. 2022).

Gene action may also be subject to population-dependent variation. For example, the length-to-width ratio QTL on chromosome 2 showed partial dominance to the 'W133' phenotype in the L1408×W133 population (Fig 5B) but switched to the 'L1408' parent allele in the L1408×W279 population (Figure 5D).

Colocalization of QTLs

Consistent with our results, previous studies evidenced colocalization of QTLs in chromosome 2 for correlated carrot root traits, including length, digital biomass, and tip fill (Turner et al. 2018). Tip fill is a related measure of the tip curvature phenotype presented here. The colocalization of QTLs may suggest shared genetic mechanisms that impact root morphology. The presence of colocalized QTLs in independent populations has been documented in maize multi-parental MAGIC populations, where specific chromosomal regions were associated with both plant height and flowering time (Michel et al. 2022).

The proximity of QTLs reported in this study, ranging from 1.2 to 3.4 Mb to those previously identified through linkage mapping and association studies on chromosome 2 (Figure 4) supports the involvement of this genomic region of chromosome 2 in shaping carrot root traits (Macko-Podgórni et al. 2017; Turner et al. 2018; Brainard et al. 2022). The presence of a shoulder curvature QTL in the L1408×W279 population, 1.7 Mb away to the estimated location of a similar shoulder trait QTL reported by Macko-Podgorni et al. (2017), adds evidence to the genetic significance of loci in chromosome 2 in root shape control (Table S4).

Brainard et al. (2022) results indicate the presence of an *OFP8-like* transcription factor less than 40 kb of a QTL identified for carrot maximum root width on chromosome 3. The QTL identified by these authors is within the 1.5 LOD interval of colocalized QTLs for tip curvature, width and length-to-width ratio identified in chromosome 3 in this study. Independent identification of genetic regions controlling root shape highlights the importance of these genomic regions in carrot root shape control.

Genetic linkage and candidate genes

Genome-wide LD in carrot diversity panels is fast decaying (Ellison et al. 2018; Brainard et al. 2022) and exhibits a non-monotonic nature (Schaid et al. 2018), but as expected for bi-parental populations, our findings suggest very slow monotonic genome-wide LD decay (Figure S11). In response to large blocks of LD, affecting QTL size precision, the candidate gene search was focused on predicted carrot genes in the *OFP-TRM* and *IQD* regulon. BLAST searches identified 41 *TRMs*, 22 *OFPs*, and 45 *IQDs* predicted genes in carrot.

Members of this plant regulon including *OFP5* and *TRM9* fell within the 1.5 LOD support interval for the length-to-width ratio QTL on chromosome 2 (Figs. 2 and 3, Table S3 and S4). The locus DCAR_007928 is a predicted repressor of elongation OFP5 and was proposed as one candidate gene for the length-to-width ratio QTL on chromosome 2 for population L1408×W133. We excluded the candidate gene DCAR_007928 from consideration in L1408×W279 as it lies outside the QTL support interval for this population. However, it is just 1.4 Mb away from the QTL region. Despite differing candidate genes, reproducibility of QTLs for both populations on chromosome 2 is supported by an overlap in the 1.5 LOD interval (15 Mb). Variation is likely due to fewer SNP markers in Population L1408×W279, precluding the identification of an SNP marker in LD at the exact physical position as in Population L1408×W133. Evidence for reproducibility of the QTL stems from overlap in physical position and identical gene action in two populations.

Predicted *TRM22*, *TRM18* and *IQD14* were also found in the support interval of significant QTLs in chromosomes 5 and 8 (Figure 3). Genes in the *TRM* and *OFP* families interact and function as transcription factors, influencing gene expression and plant organ shape in tomato and Arabidopsis (Snouffer et al. 2020; Li et al. 2023). The *IQD* pathway also encodes proteins that regulate cell proliferation and expansion, contributing to fruit shape determination (Wendrich et al. 2018; Yang et al. 2020).

OFP5 and *OFP8* homologs found in carrots are predicted repressors of elongation (Table S4). In addition, Arabidopsis orthologs *AtOFP5*, *AtOFP8* and *AtOFP13* have been confirmed as repressors of organ elongation (Wang et al. 2007, Wang et al. 2011; Zhang et al. 2020). In tomatoes, *TRM9*, *TRM18*, and *TRM22* have been associated with cellular organization and shoot outgrowth which may suggest their role in modulating phytohormones (Namphengsone, 2019).

Although the *OFP-TRM* and *IQD* regulon has been recognized as a master regulator of shape in fruit, grains, and potato tubers (Wu et al. 2018; Guo et al. 2020; Li et al. 2023), its involvement in roots has been limited to one study in radish (*Raphanus sativus,* Wang et al. 2020). The present study is the first linkage mapping report connecting the *OFP-TRM* and *IQD* regulon to carrot root traits that constitute market class.

The influence of the established mechanisms of the *OFP-TRM* and *IQD* plant regulon on carrot root shape remains uncertain. This ambiguity arises from the composition of carrot roots, comprising both root and hypocotyl tissue originating from secondary growth of cambium with parenchyma tissues. Carrot roots have swollen and expanded xylem and phloem tissues beyond the primary vascular tissues (Goldman, 2020) which contrasts with the division patterns and cell arrangement of fruit tissue. Nevertheless, the extension of the *OFP-TRM* and *IQD* regulon's influence beyond fruit shape has been well demonstrated in potato (*Solanum tuberosum* L.) tubers, which are a modified stem. Back in 1994, van Eck et al. identified the *Ro* locus, responsible for round tuber shape, on chromosome 10. Studies subsequently found QTLs for tuber shape mapping to the same locus in diploid potato F_2 populations (Endelman and Jansky 2016) and molecular markers were developed for the locus (Chen et al. 2019). In 2018, Wu et al. conducted fine mapping of the *Ro* locus and confirmed that the potato *Ro* locus is controlled by *StOFP20,* an ortholog of tomato *SlOFP20*. The function of *StOFP20* and its interaction with *TRM* members was later experimentally confirmed by Ju et al. (2023).

Although we limited our search for candidate genes to the *OFP-TRM* and *IQD* plant shape regulon, other families of genes may also contribute to root shape control. Our large linkage blocks include the possibility of harboring genes in other pathways previously reported to be involved in carrot root formation such as the *AT-hook containing nuclear localized (AHL)* gene family or other undiscovered gene families. *DcAHLc1,* for example is a member of the *AHL* gene family and was proposed as a candidate for carrot root formation (Macko-Podgórni et al. 2017). Members of the *AHL* gene family also fell within QTL confidence intervals controlling root shape in mapping studies (Turner et al. 2018). Further characterization of the *AHL* family in carrots has demonstrated that their role is mainly in plant growth and storage root development (Machaj and Grzebelus, 2020), which opens up the possibility that multiple mechanisms may be responsible for root development and shape patterning of carrots.

Genetic mapping in carrots

Although inbred lines with 99.6 % homozygosity have been reported (Wang et al. 2023), the outcrossing mating system of carrots presents challenges in obtaining homozygous inbred lines. Inbreeding depression also tends to result in lines with genetic heterogeneity that show uniform and stable phenotypes in self- or sib-mated lines (Rubatzky et al. 1999; Simon, 2021). This is compounded by patterns of segregation distortion observed in chromosomes 1, 4, 8, and 9 (Grzebelus et al. 2014; Iorizzo et al. 2019; Bannoud et al. 2019). Limited availability of homozygous inbred lines complicates the linkage mapping problem. To overcome these limitations, doubled haploid research has gained attention (Andersen et al. 1990; Meyer et al. 2022), offering potential avenues for carrot mapping and breeding. Searching alleles that provide inbreeding resistance in carrots, along with reproducible genotyping technologies and high-quality telomere-to-telomere genome assemblies, has the potential to advance breeding and mapping efforts for of agronomically and horticulturally important traits in carrot.

This mapping study provides insights into the genetic basis of root shape traits associated with carrot market class, indicating a potential link with the *OPF-TRM* and *IQD* regulon, which has been well established in tuber and aerial plant organ shape (Wu et al. 2018) but with very limited focus on root traits. A better understanding of genetic shape control in carrot roots may enhance the development of improved varieties, expanding current carrot market classes.

Data Availability Statement

SNP markers filtered for MAF>=0.05, Depth of 20 for 95% of the population and only bi-allelic sites are provided as VCF files along with linkage maps that include phenotypes. Excel files with phenotypes computed from digital pipelines and annotated R scripts used to create linkage maps and to summarize phenotypic datasets are available in https://zenodo.org/records/10023296 (DOI: 10.5281/zenodo.10023295). Supplemental Materials are available locally at https://zenodo.org/records/10626038 (DOI: 10.5281/zenodo.10257998). Supplemental Figures includes Figures S1 to S12. Supplemental Table includes Tables S1 through S4. File S1 includes multiple sequence alignment to conserved Tonneu Recruiting Motifs (TRM) for four previously uncharacterized predicted carrot genes DCAR_008585 (LOC108208046), DCAR_017186 (LOC108220104), DCAR_021448 (LOC108228003) and DCAR_027681 (LOC108200088). File S2 includes amino acid sequences of know regulators of shape in tomato (*Solanum lycopersicum*) and predicted genes in carrot *(Daucus carota* var. *sativus*) with sequence homology to the shape regulon *OFP-TRM* and IQD for assembly, GCA_001625215.1, bioproject PRJNA268187. Visual representation of the relationships among gene sequences of carrot and tomato *TRMs* homologs are presented in Figure S12.

Acknowledgements

The authors thank Ashley Snouffer for guidance on amino acid sequence BLAST search and Sean Fenstemaker for their guidance with genetic mapping.

Funding

This work was supported in part by the National Science Foundation's Plant Genome Research Project, under award number 2048425.

Conflict of Interest

None declared.

References

Aballay MM, Aguirre NC, Filippi CV, Valentini GH, Sánchez G. 2021. Fine-tuning the performance of ddRAD-seq in the peach genome. Sci Rep 11:6298. doi: https://doi.org/10.1038/s41598-021-85815-0

Andersen SB, Christiansen I, Farestveit B. 1990. Carrot (*Daucus carota* L.): In Vitro Production of Haploids and Field Trials. In: Bajaj YPS (ed) Haploids in Crop Improvement I. Springer, Berlin. 393-402. doi: https://doi.org/10.1007/978-3-642-61499-6_20

Banga O. 1957. Origin of the European cultivated carrot. Instituut voor de Veredeling van Tuinbouwgewassen. doi: https://doi.org/10.1007/BF00179518

Banga O. 1963a. Main Types of the Western Carotene Carrot and their Origin. Main Types of the Western Carotene Carrot and their Origin. W.E.J. Tjeenk Willink. Ithacca, NY.

Banga O. 1963b. Origin and distribution of the western cultivated carrot. Genet Agrar 17:357-370.

Bannoud F, Ellison S, Paolinelli M, Horejsi T, Senalik D, Fanzone M, Iorizzo M, Simon PW, Cavagnaro PF. 2019. Dissecting the genetic control of root and leaf tissue-specific anthocyanin pigmentation in carrot (*Daucus carota* L.). Theor App Genet 132:2485-2507. doi: https://doi.org/10.1007/s00122-019-03366-5

Bates D, Mächler M, Bolker B, Walker S. 2015. Fitting Linear Mixed-Effects Models Using lme4. J of Statistical Softw 67:1-48. doi: https://doi.org/10.18637/jss.v067.i01

Brainard SH, Bustamante JA, Dawson JC, Spalding EP, Goldman IL. 2021. A digital image-based phenotyping platform for analyzing root shape attributes in carrot. Front Plant Sci 12:1171. doi: https://doi.org/10.3389/fpls.2021.690031

Brainard SH, Ellison SL, Simon PW, Dawson JC, Goldman IL. 2022. Genetic characterization of carrot root shape and size using genome-wide association analysis and genomic-estimated breeding values Theor Appl Genet 135(2):605-622. doi: https://doi.org/10.1007/s00122-021-03988-8

Braun SR, Endelman JB, Haynes KG, Jansky SH. 2017. Quantitative Trait Loci for Resistance to Common Scab and Cold-Induced Sweetening in Diploid Potato. The Plant Genome 10:2016. doi: https://doi.org/10.3835/plantgenome2016.10.0110

Broman K. 2023. qtl manual. https://rqtl.org/manual/qtl-manual.pdf. Accessed June 14 2023

Bürstenbinder K, Möller B, Plötner R, Stamm G, Hause G, Mitra D, Abel S. 2017. The IQD Family of Calmodulin-Binding Proteins Links Calcium Signaling to Microtubules, Membrane Subdomains, and the Nucleus. Plant Physiol 173:1692-1708. doi: https://doi.org/10.1104/pp.16.01743

Chen N, Zhu W, Xu J, Duan S, Bian C, Hu J, Wang W, Li G, Jin L. 2019. Molecular marker development and primary physical map construction for the tuber shape Ro gene locus in diploid potato (Solanum tuberosum L.). Mol Breed 39:1-9. doi: https://doi.org/10.1007/s11032-018-0913-z

Coe K, Bostan H, Rolling W, Turner-Hissong S, Macko-Podgórni A, Senalik D, Liu S, Seth R, Curaba J, Mengist MF, Grzebelus, D, Van Deynze A, Dawson J, Ellison S, Simon PW, Iorizzo, M. 2023. Population genomics identifies genetic signatures of carrot domestication and improvement and uncovers the origin of high-carotenoid orange carrots. Nature Plants 9:1643–1658. doi: https://doi.org/10.1038/s41477-023-01526-6

Colquhoun JB, Heider DJ, Rittmeyer RA. 2019. Transplanted Leek Herbicide Efficacy - Muck Soil. https://specialtycrops.wisc.edu/integrated-weed-management/#research-reports. Accessed 17 Feb 2023

Ellison S. 2019. Carrot domestication. In: Simon P, Iorizzo M, Grzebelus D, Baranski R (eds). The carrot genome. Springer. Cham, Switzerland. doi: https://doi.org/10.1007/978-3-030-03389-7_5.

Ellison S, Senalik D, Bostan H, Iorizzo M, Simon P. 2017. Fine mapping, transcriptome analysis, and marker development for Y2, the gene that conditions β-carotene accumulation in carrot (Daucus carota L.). G3: Genes, Genomes, Genetics:7(8):2665-2675. Doi: https://doi.org/10.1534/g3.117.043067

Ellison S, Luby CH, Corak KE, Coe KM, Senalik D, Iorizzo M, Goldman IL, Simon PW, Dawson JC. 2018. Carotenoid Presence Is Associated with the Or Gene in Domesticated Carrot. Genetics 210(4):1497-1508. doi: https://doi.org/10.1534/genetics.118.301299

Elshire RJ, Glaubitz JC, Sun Q, Poland JA, Kawamoto K, Buckler ES, et al. 2011. A robust, simple genotyping-by-sequencing (GBS) approach for high diversity species. PloS One, 6(5):e19379. doi: https://doi.org/10.1371/journal.pone.0019379

Endelman JB. 2023. MapRtools: Tools for genetic mapping teaching and research (R package version 0.30). https://github.com/jendelman/MapRtools/. Accessed 17 May 2023.

Endelman JB, Jansky SH. 2016. Genetic mapping with an inbred line-derived F2 population in potato. Theor Appl Genet 129:935-943. doi: https://doi.org/10.1007/s00122-016-2673-7

Geoffriau E, Simon PW. 2020. Carrots and related Apiaceae crops Vol 33. CABI, Oxfordshire, UK.

Glaubitz JC, Casstevens TM, Lu F, Harriman J, Elshire RJ, Sun Q, Buckler ES. 2014. TASSEL-GBS: a high capacity genotyping by sequencing analysis pipeline. PloS one 9(2): e90346. doi: https://doi.org/10.1371/journal.pone.0090346

Glémin S, Bazin E, Charlesworth D. 2006. Impact of mating systems on patterns of sequence polymorphism in flowering plants. Proc R Soc B Biol Sci. 273:1604 doi: https://doi.org/10.1098/rspb.2006.3657

Goldman IL. 1996. A list of germplasm releases from the University of Wisconsin carrot breeding program, 1964–1994. HortScience 31(5):882-883. doi: https://doi.org/10.21273/HORTSCI.31.5.882

Goldman IL. 2020. The root vegetables: beet, carrot, parsnip, and turnip. In: H. C. Wien and H. Stutzel. The Physiology of Vegetable Crops. 2nd edn. Boston, Massachusetts CABI. doi: https://doi.org/10.1079/9781786393777.0399

Grzebelus D, Iorizzo M, Senalik D, Ellison S, Cavagnaro P, Macko-Podgorni A, Heller-Uszynska K, Kilian A, Nothnagel T, Allender C. 2014. Diversity, genetic mapping, and signatures of domestication in the carrot (*Daucus carota* L.) genome, as revealed by Diversity Arrays Technology (DArT) markers. Mol Breed 3:625-637. doi: https://doi.org/10.1007/s11032-013-9979-9

Guo C, Zhou J, Li D. 2021. New insights into functions of IQ67-domain proteins. Front in Plant Sci 11:614851. doi: https://doi.org/10.3389/fpls.2020.614851

Holland JB. 2007. Genetic architecture of complex traits in plants. Curr Opin Plant Biol. 10(2):156-161. doi: https://doi.org/10.1016/j.pbi.2007.01.003

Iorizzo M, Ellison S, Pottorff M, Cavagnaro PF. 2019. In: Simon P, Iorizzo M, Grzebelus D, Baranski R. The carrot genome. Springer Cham. doi: https://doi.org/10.1007/978-3-030-03389-7_5

Iorizzo M, Ellison S, Senalik D, Zeng P, Satapoomin P, Huang J, Bowman M, Iovene M, Sanseverino W, Cavagnaro P, Yildiz M, Macko-Podgórni A, Moranska E, Grzebelus E, Grzebelus D, Ashrafi H, Zheng Z, Cheng S, Spooner D, Van Deynze A, Simon PW. 2016. A high-quality carrot genome assembly provides new insights into carotenoid accumulation and asterid genome evolution. Nat Genet 48(6):657-666. doi: https://doi.org/10.1038/ng.3565

Iorizzo M, Senalik DA, Ellison SL, Grzebelus D, Cavagnaro PF, Allender C, Brunet J, Spooner DM, Van Deynze A, Simon PW. 2013. Genetic structure and domestication of carrot (Daucus carota subsp. sativus) (Apiaceae). Am J Bot 100(5):930-938. doi: https://doi.org/10.3732/ajb.1300055

Ju A, Ye W, Yan Y, Li C, Wei L, Ling MA, Shang Y, Gao D. 2023. StOFP20 regulates tuber shape and interacts with TONNEAU1 Recruiting Motif proteins in potato. J of Integr Agric. 22(3):752-761. doi: https://doi.org/10.1016/j.jia.2022.08.069

Kosambi DD. 1943. The estimation of map distances from recombination values. Ann Eugen 12:172–175. doi: https://doi.org/10.1111/j.1469-1809.1943.tb02321

Lazzaro MD, Wu S, Snouffer A, Wang Y, van der Knaap E. 2018. Plant Organ Shapes Are Regulated by Protein Interactions and Associations With Microtubules. Front Plant Sci 9:1766. doi: https://doi.org/10.3389/fpls.2018.01766

Lenth RV. 2020. emmeans: Estimated marginal means, aka least-squares means. R package version 1.5.4.1. https://CRAN.R-project.org/package=emmeans. Accessed Mar 15 2023.

Li H. 2011. A statistical framework for SNP calling, mutation discovery, association mapping and population genetical parameter estimation from sequencing data. Bioinformatics 27(21):2987-93. doi: https://doi.org/10.1093/bioinformatics/btr509

Li Q, Luo S, Zhang L, Feng Q, Song L, Sapkota M, Xuan S, Wang Y, Zhao J, van der Knaap E. 2023. Molecular and genetic regulations of fleshy fruit shape and lessons from Arabidopsis and rice. Horticulture Research. doi: https://doi.org/10.1093/hr/uhad108

Lucier G, Lin B. 2007. Factors affecting carrot consumption in the United States. https://naldc.nal.usda.gov/catalog/41113. Accessed Mar 15 2023.

Machaj G, Grzebelus D. 2020 Characteristics of the AT-hook motif containing nuclear localized (AHL) genes in carrot provides insight into their role in plant growth and storage root development. Genes 12(5):764. doi: https://doi.org/10.3390/genes12050764

Magruder, R., V.R. Boswel, S.L. Emsweller, J.C. Miller, A.E. Hutchins, J.F. Wood, M.M. Parker, and H.H. Zimmerley. 1940. Descriptions of types of principal American varieties of orange-fleshed carrots. U.S. Department of Agriculture 354.

Macko-Podgórni A, Machaj G, Stelmach K, Senalik D, Grzebelus E, Iorizzo M, Simon PW, Grzebelus D. 2017. Characterization of a genomic region under selection in cultivated carrot (*Daucus carota* subsp. *sativus*) reveals a candidate domestication gene. Front in Plant Sci 8:12. doi: https://doi.org/10.3389/fpls.2017.00012

Meyer CM, Goldman IL, Grzebelus E, Krysan PJ. 2022. Efficient production of transgene-free, gene-edited carrot plants via protoplast transformation. Plant Cell Rep 41(4):947-960. doi: https://doi.org/10.1007/s00299-022-02830-9

Michel KJ, Lima DC, Hundley H, Singan V, Yoshinaga Y, Daum C, et al. 2022. Genetic mapping and prediction of flowering time and plant height in a maize stiff stalk MAGIC population. Genetics 221(2):iyac063. doi: https://doi.org/10.1093/genetics/iyac063

Mou B. 2022. Vegetable Cultivar Descriptions for North America List 28 HortScience 57(8):949-1040. doi: https://doi.org/10.21273/HORTSCI.57.8.949

Myles S, Peiffer J, Brown PJ, Ersoz ES, Zhang Z, Costich DE, Buckler ES. 2009. Association mapping: critical considerations shift from genotyping to experimental design. Plant Cell 21(8):2194-2202. doi: https://doi.org/10.1105/tpc.109.068437

Namphengsone N. 2019. The Role of OFPs and TRMs in Organogenesis. Dissertation. The University of Kansas.

Pan, Y., X. Liang, M. Gao, H. Liu, H. Meng, Y. Weng, and Z. Cheng. 2017. Round fruit shape in WI7239 cucumber is controlled by two interacting quantitative trait loci with one putatively encoding a tomato SUN homolog. Theor Appl Genet 130(3):573-586. doi: https://doi.org/10.1007/s00122-016-2836-6

Parsons J, Matthews W, Iorizzo M, Roberts P, Simon P. 2015. Meloidogyne incognita nematode resistance QTL in carrot. Mol Breed 35:1-11. doi: https://doi.org/10.1007/s11032-015-0309-2

Piepho H, Möhring J, Schulz-Streeck T, Ogutu JO. 2012. A stage-wise approach for the analysis of multi-environment trials. Biom J 54(6):844-860. doi: https://doi.org/10.1002/bimj.201100219

R Core Team. 2022. R-4.2.2. R Foundation for Statistical Computing, Vienna, Austria. https://cran.r-project.org/bin/windows/base/. Accessed 06 June 2023.

Rong J, Janson S, Umehara M, Ono M, Vrieling K. 2010. Historical and contemporary gene dispersal in wild carrot (Daucus carota ssp. carota) populations. Ann Bot 106(2): 285-296. doi: https://doi.org/10.1093/aob/mcq108

Rubatzky VE, Quiros CF, Simon PW. 1999. Carrots and related vegetable Umbelliferae. CABI publishing, New York, NY, USA.

Schaefer S, Belcram B, Uyttewaal U, Duroc D, Goussot G, Legland L, Laruelle L, de Tauzia-Moreau de Tauzia-Moreau, Pastuglia P, Bouchez B. 2017. The preprophase band of microtubules controls the robustness of division orientation in plants. Science. 356(6334):186-189. doi: https://doi.org/10.1126/science.aal3016

Schaid DJ, Chen W, Larson NB. 2018. From genome-wide associations to candidate causal variants by statistical fine-mapping. Nat Rev Genet 19(8):491-504. doi: https://doi.org/10.1038/s41576-018-0016-z

Simon PW. 2021. Carrot (*Daucus carota* L.) breeding. Advances in Plant Breeding Strategies: Vegetable Crops: Volume 8: Bulbs, Roots and Tubers. doi: https://doi.org/10.1007/978-3-030-66965-2_5

Snouffer A, Kraus C, van der Knaap E. 2020. The shape of things to come: ovate family proteins regulate plant organ shape. Curr Opin Plant Biol 53:98-105. doi: https://doi.org/10.1016/j.pbi.2019.10.005

Timothy L. Bailey and Michael Gribskov. 1998. Combining evidence using p-values: application to sequence homology searches Bioinformatics 14(1):48-54. doi: https://doi.org/10.1093/bioinformatics/14.1.48

Turner SD, Ellison SL, Senalik DA, Simon PW, Spalding EP, Miller ND. 2018. An automated image analysis pipeline enables genetic studies of shoot and root morphology in carrot (*Daucus carota* L.). Front Plant Sci 9:1703. doi: https://doi.org/10.3389/fpls.2018.01703

USDA National Cooperative Soil Survey .2021. Houghton Series. https://soilseries.sc.egov.usda.gov/OSD_Docs/H/HOUGHTON.html#:~:text=The%20Houghton%20series%20consists%20of,from%200%20to%202%20percent. Accessed 17 February 2023

USDA National Agricultural Statistics Service. 2023. Statistics by Subject: Carrots. https://www.nass.usda.gov/Statistics_by_Subject/result.php?E5E0113F-5080-388E-BC70-52E2C8BD18AE&sector=CROPS&group=VEGETABLES&comm=CARROTS. Accessed 15 September 2023

van der Knaap E, Chakrabarti M, Chu YH, Clevenger JP, Illa-Berenguer E, Huang Z, Keyhaninejad N, Mu Q, Sun L, Wang Y. 2014. What lies beyond the eye: the molecular mechanisms regulating tomato fruit weight and shape. Front Plat Sci 5:227. doi: https://doi.org/10.3389/fpls.2014.00227

van der Knaap E, Østergaard L. 2018. Shaping a fruit: Developmental pathways that impact growth patterns. Semin Cell Dev Biol 79:27-36. doi: https://doi.org/10.1016/j.semcdb.2017.10.028

van Eck HJ, Jacobs JM, Stam P, Ton J, Stiekema WJ, and Jacobsen E. 1994. Multiple alleles for tuber shape in diploid potato detected by qualitative and quantitative genetic analysis using RFLPs. Genetics 137(1):303-309. doi: https://doi.org/10.1093/genetics/137.1.303

Vega A, Goldman IL. 2023. Planting Density Does Not Affect Root Shape Traits Associated With Market Class in Carrot. HortScience, 58(9), 996-1004. doi: https://doi.org/10.21273/HORTSCI17232-23

Wang S, Chang Y, Guo J, Chen J. 2007. Arabidopsis Ovate Family Protein 1 is a transcriptional repressor that suppresses cell elongation. The Plant J. 50(5):858-872 doi: https://doi.org/10.1111/j.1365-313X.2007.03096.x

Wang S, Chang Y, Guo J, Zeng Q, Ellis BE, Chen J. 2011. Arabidopsis ovate family proteins, a novel transcriptional repressor family, control multiple aspects of plant growth and development. PLoS One. 6(8):e23896. doi: https://doi.org/10.1371/journal.pone.0023896

Wang Y, Liu P, Liu H, Zhang R, Liang Y, Xu Z, Li X, Luo Q, Tan G, Wang G. 2023. Telomere-to-telomere carrot (Daucus carota) genome assembly reveals carotenoid characteristics. Hortic Res uhad103. doi: https://doi.org/10.1093/hr/uhad103

Wang Y, Wang Q, Hao W, Sun H, Zhang L. 2020. Characterization of the OFP gene family and its putative involvement of tuberous root shape in radish. International J Molr Sci 21(4):1293. doi: https://doi.org/10.3390/ijms21041293

Wendrich JR, Yang BJ, Mijnhout P, Xue HW, De Rybel B, Weijers D. 2018. IQD proteins integrate auxin and calcium signaling to regulate microtubule dynamics during Arabidopsis development. bioRxiv. doi: https://doi.org/10.1101/275560

Wu S, Zhang B, Keyhaninejad N, Rodríguez GR, Kim HJ, Chakrabarti M, Illa-Berenguer E, Taitano NK, Gonzalo MJ, Díaz A, Pan Y, Leisner CP, Halterman D, Buell CR, Weng Y, Jansky SH, van Eck H, Willemsen J, Monforte AJ, Meulia T, van der Knaap E. 2018. A common genetic mechanism underlies morphological diversity in fruits and other plant organs. Nat Commun 9(1):4734. doi: https://doi.org/10.1038/s41467-018-07216-8

Yang B, Wendrich JR, De Rybel B, Weijers D, Xue H. 2020. Rice microtubule-associated protein IQ67-DOMAIN14 regulates grain shape by modulating microtubule cytoskeleton dynamics. Plant Biotechnol J. 8(5):141-1152. doi: https://doi.org/10.1111/pbi.13279

Zhang L, Azhar MT, Che J, Shang H. 2022. Genome-wide identification, expression and evolution analysis of OVATE family proteins in cotton (Gossypium spp.). Gene 834:146653. doi: https://doi.org/10.1016/j.gene.2022.146653

Zhang X, Wu J, Yu Q, Liu R, Wang Z, Sun Y. 2020. AtOFPs regulate cell elongation by modulating microtubule orientation via direct interaction with TONNEAU2. Plant Sci 292, 110405. doi: https://doi.org/10.1016/j.plantsci.2020.110405

Zhao D, Li Q, Zhang C, Zhang C, Yang Q, Pan L, Ren X, Lu J, Gu M, Liu Q. 2018. GS9 acts as a transcriptional activator to regulate rice grain shape and appearance quality. Nat Commun 9(1):1240. doi: https://doi.org/10.1038/

Tables

Table 1. Variance partitioning and broad-sense heritability (H^2) on an entry-mean basis for root shape traits in the carrot mapping populations L1408×W133 and L1408×W279 in a two-year field trial.

Source	*Variance components*					
	Shoulder curvature (PC-score)	Tip curvature (PC-score)	Biomass (m^2)	Width (mm)	Length (mm)	Length-to-width ratio
	Population L1408×W133					
Year (Y)	0.18	1.82	0.003	5.66	281	1.58
Genotype (G)	0.51	0.56	0.225	3.75	498	1.43
G × Y	0.08	0.36	0.059	1.10	0	0.28
Block/Y	0	0	0.011	0.07	15	0.03
Residual	0.59	1.84	0.401	4.41	639	0.97
	Broad-sense heritability					
	0.73	0.46	0.63	0.69	0.75	0.79
	Population L1408×W279					
Year	0.87	1.87	0.199	11.36	78	1.67
Genotype	0.31	1.25	0.183	5.20	516	2.21
G × Y	0.02	0.13	0.032	1.55	8	0.61
Block/Y	0.01	0.01	0.000	0.08	0	0.01
Residual	0.94	4.07	0.531	5.65	781	0.96
	Broad-sense heritability					
	0.56	0.54	0.55	0.70	0.72	0.80

Table 2. Summary statistics of the linkage maps for carrot $F_{2:3}$ mapping populations L1408×W133 (n=119) and L1408×W279 (n=128).

Chromosome	Number of markers	Map statistics (cM)		
		Length	Average spacing	Maximum spacing
Population L1408×W133				
1	548	135.9	0.2	6.5
2	267	97.5	0.4	7.3
3	275	96.4	0.4	8.2
4	140	62.4	0.4	6.0
5	219	89.6	0.4	10.1
6	296	52.4	0.2	5.7
7	121	72.7	0.6	8.3
8	186	37.5	0.2	5.0
9	98	46.0	0.5	5.5
Overall	2150	690.4	0.3	10.1
Population L1408×W279				
1	31	53.0	1.8	11.7
2	30	42.0	1.4	7.4
3	62	74.5	1.2	13.5
4	70	31.7	0.5	6.2
5	37	32.3	0.9	4.7
6	26	45.1	1.8	11.9
7	45	20.5	0.5	5.8
8	24	69.6	3.0	22.5
9	16	37.5	2.5	7.8
Overall	341	406.2	1.2	22.5

List of figure captions

Figure 1 Photograph of carrot (*D. carota* var *sativus*) founders 'L1408', 'W133', and 'W279' (**A**). Boxplots displaying differences in carrot root shape traits among founders: (**B**) shoulder curvature, (**C**) tip curvature, (**D**) length, (**E**) length-to-width ratio, (**F**) width, and (**G**) biomass. Significance of mean differences is indicated by distinct lowercase letters within each boxplot (α=0.05). Multiple comparisons were corrected using the Šidák correction.

Figure 2 Phenotypic correlations between populations for root shape traits. Scatterplots of Best Linear Unbiased Estimates (BLUEs) below the diagonal show the relationship between traits for both populations. Pearson correlations (r) are shown above the diagonal for each population. The diagonal is the distribution of the trait for each population. All correlations were found to be significant at α=0.05, except for the correlations between biomass and length-to-width ratio, biomass and tip curvature, biomass and shoulder curvature, as well as length and width. LW = length-to-width.

Figure 3 Composite interval mapping (CIM) of root shape traits in the $F_{2:3}$ L1408xW133 (**a**) and L1408xW279 mapping populations (**b**). The y-axis represents the logarithm of odds (LOD). The LOD significance threshold (α=0.05, 1000 permutations) for each variable is indicated by the horizontal lines of the same color. The annotated known position of predicted carrot proteins associated with biological shape within the 1.5-LOD support interval, and less than 2 Mb of significant QTLs are represented by black vertical dotted lines in each chromosome and annotated. *OFPs* are *OVATE Family Proteins, TRMs* are *TONNEAU1 Recruiting Motif* and *IQDs* are IQ67 domain. The x-axis represents the genetic position (cM) across nine chromosomes.

Figure 4 Reproducible QTL peaks identified for length-to-width ratio on chromosome 2 and root width on chromosome 6 in $F_{2:3}$ mapping populations L1408xW133 (**A**) and L1408xW279 (**B**). Dashed black vertical lines indicate annotated positions of predicted regulators of shape in carrots, namely OVATE Family Proteins 5 (*OFP5*) and TONNEAU1 Recruiting Motif 9 (*TRM9*). Additionally, dashed red vertical lines mark the approximate locations of previously reported chromosomal regions (QTLs) associated with carrot root shape traits (Brainard et al. 2022; Turner et al., 2018; Macko-Podgórni et al. 2017). The x-axis represents the physical position in Mega bases (Mb) across chromosomes 2 and 6.

Figure 5 Relationship between genotype at SNP loci of reproducible QTLs for width (mm) and length-to-width ratio in carrot $F_{2:3}$ populations L1408×W133 (n=119) and L1408×W279 (n=128). Effect plots for width (**A**) and length-to-width ratio (**B**) in population L1408×W133. Effect plots for width (**C**) and length-to-width ratio (**D**) in validation population L1408×W279. Genotypes 'A' (L1408) and 'B' (W133 or W279) represent the two homozygous states, while 'H' denotes the heterozygote. Boxplots with different uppercase letters indicate significant differences at α=0.05. Multiple comparisons were corrected using the Šidák correction.

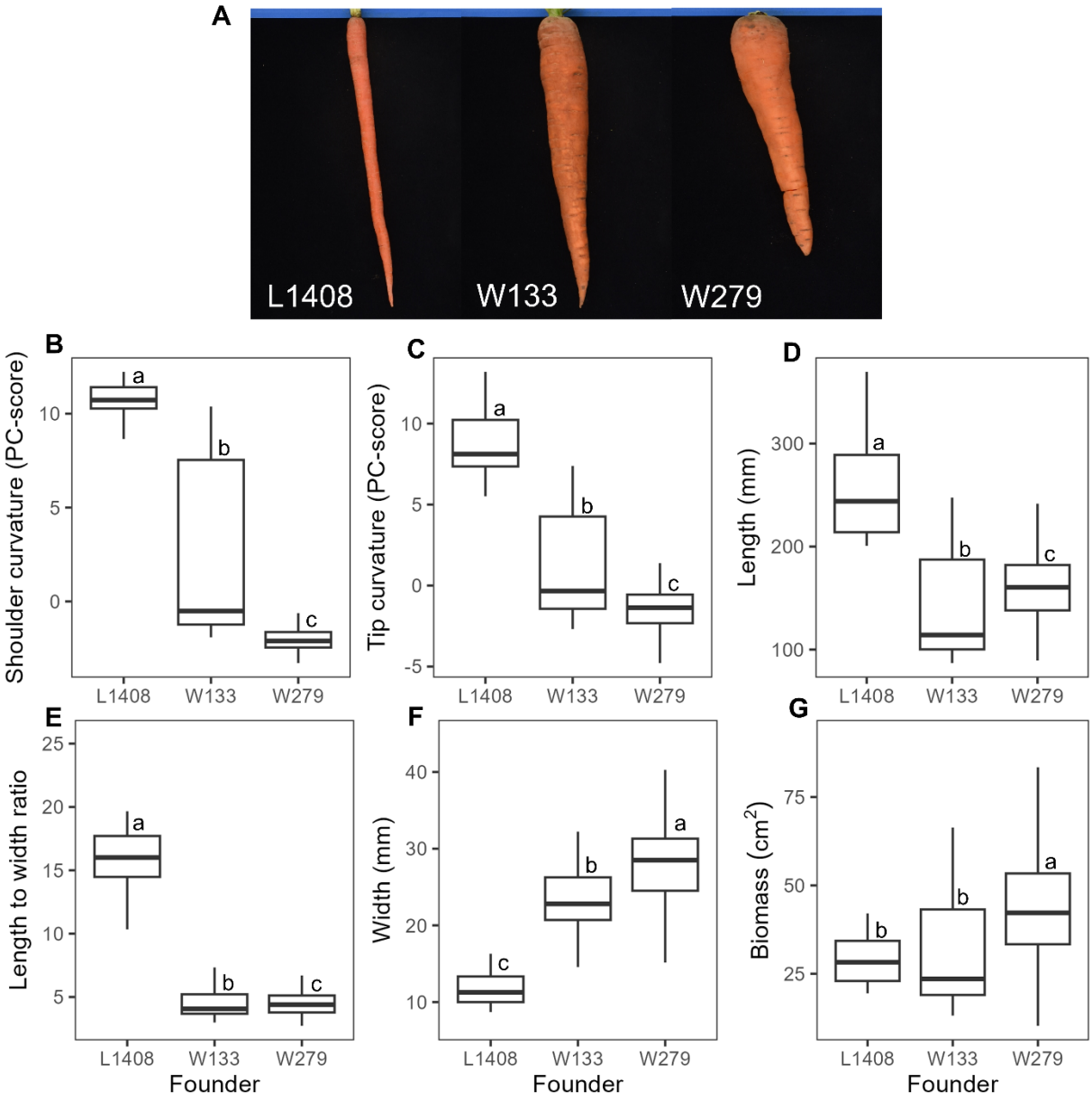

Figure 1
165x165 mm (x DPI)

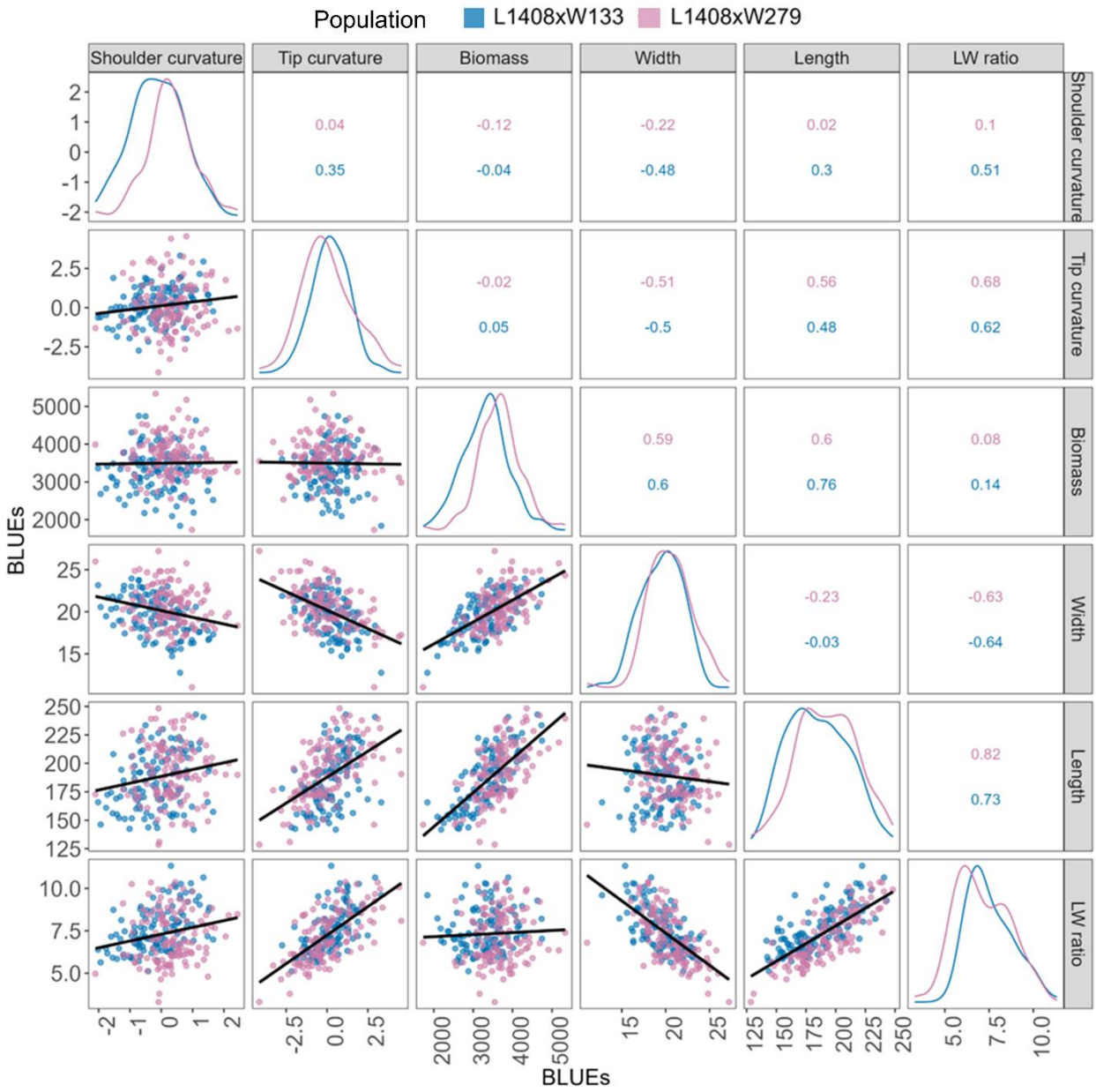

Figure 2
165x165 mm (x DPI)

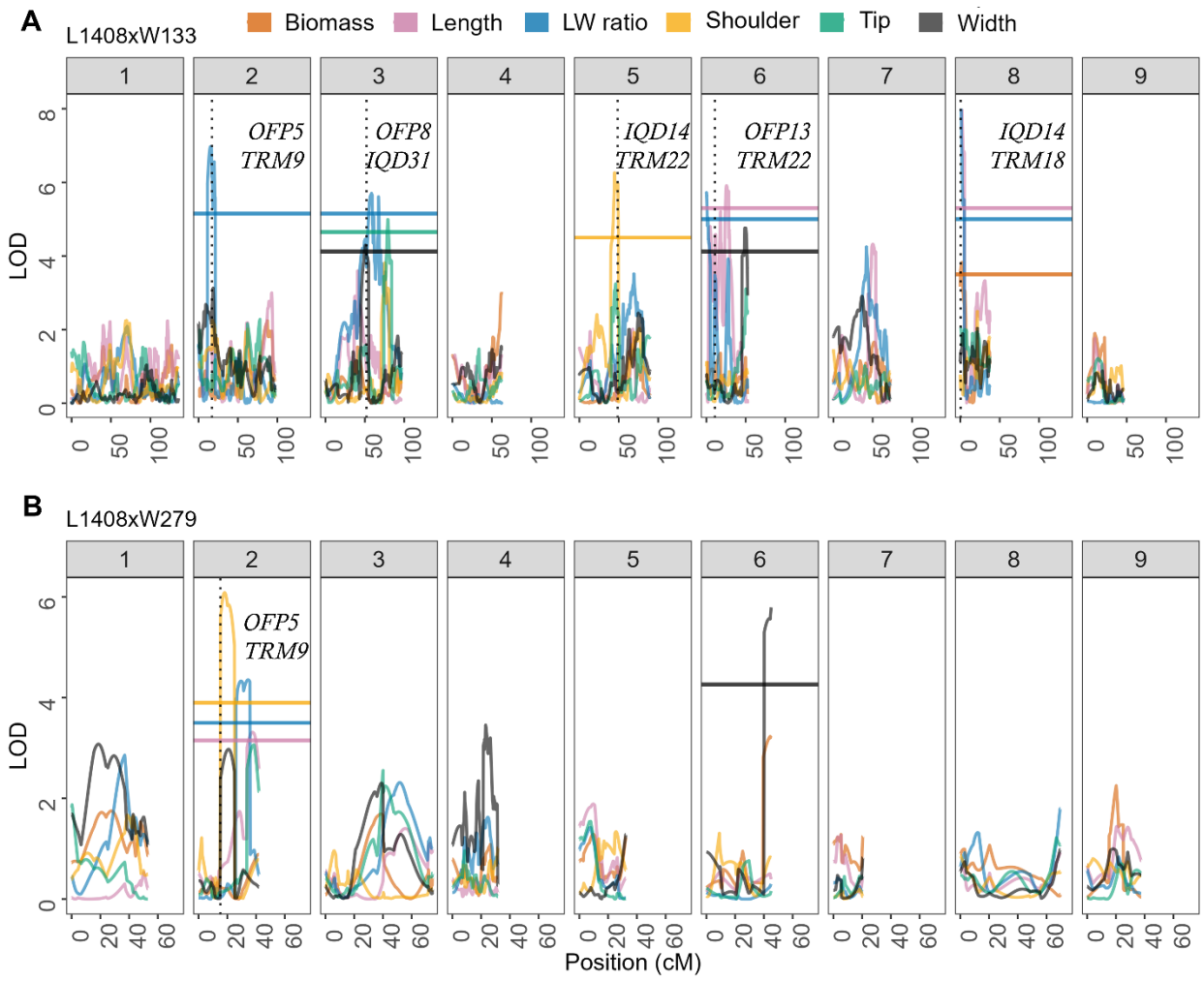

Figure 3
165x136 mm (x DPI)

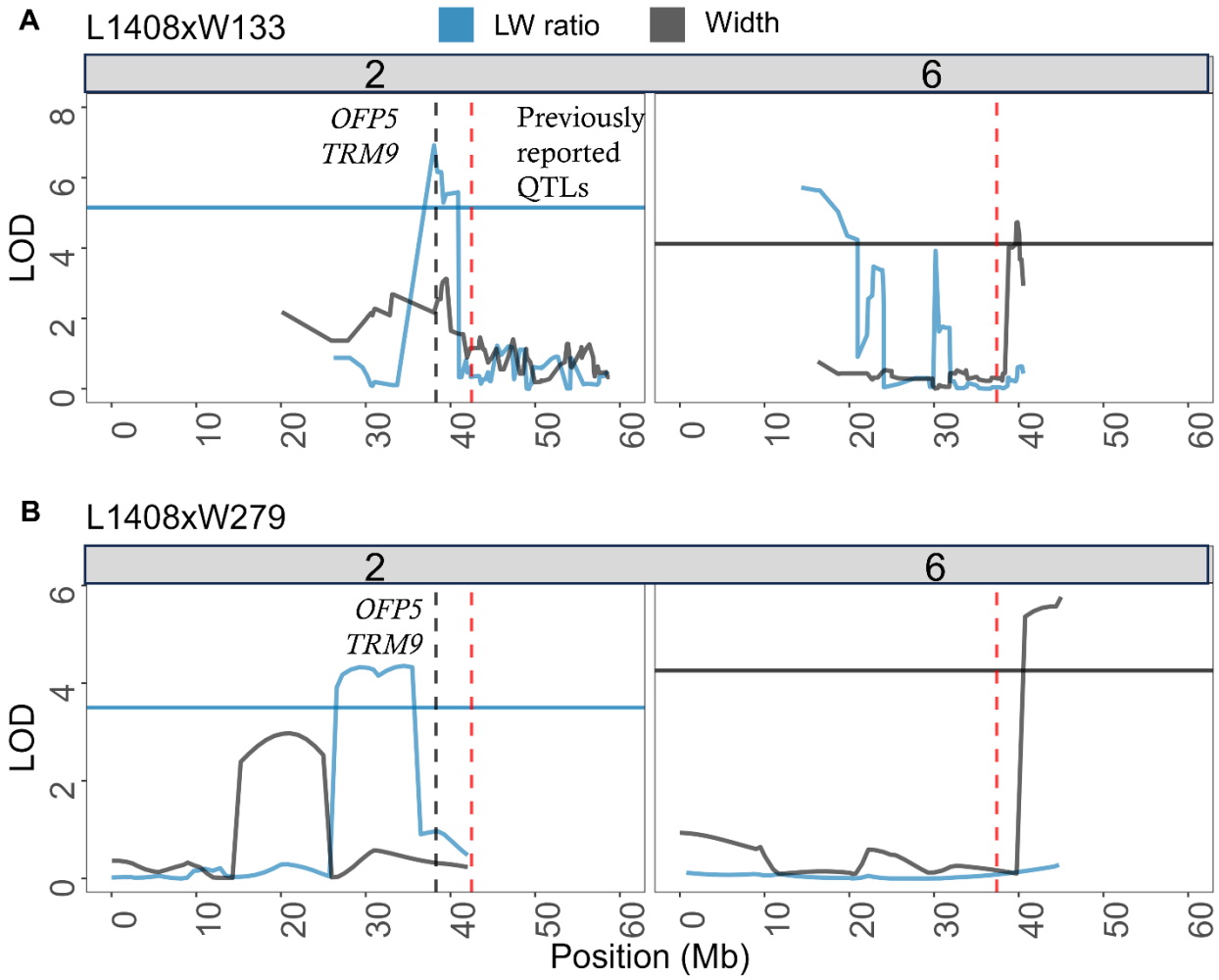

Figure 4
165x135 mm (x DPI)

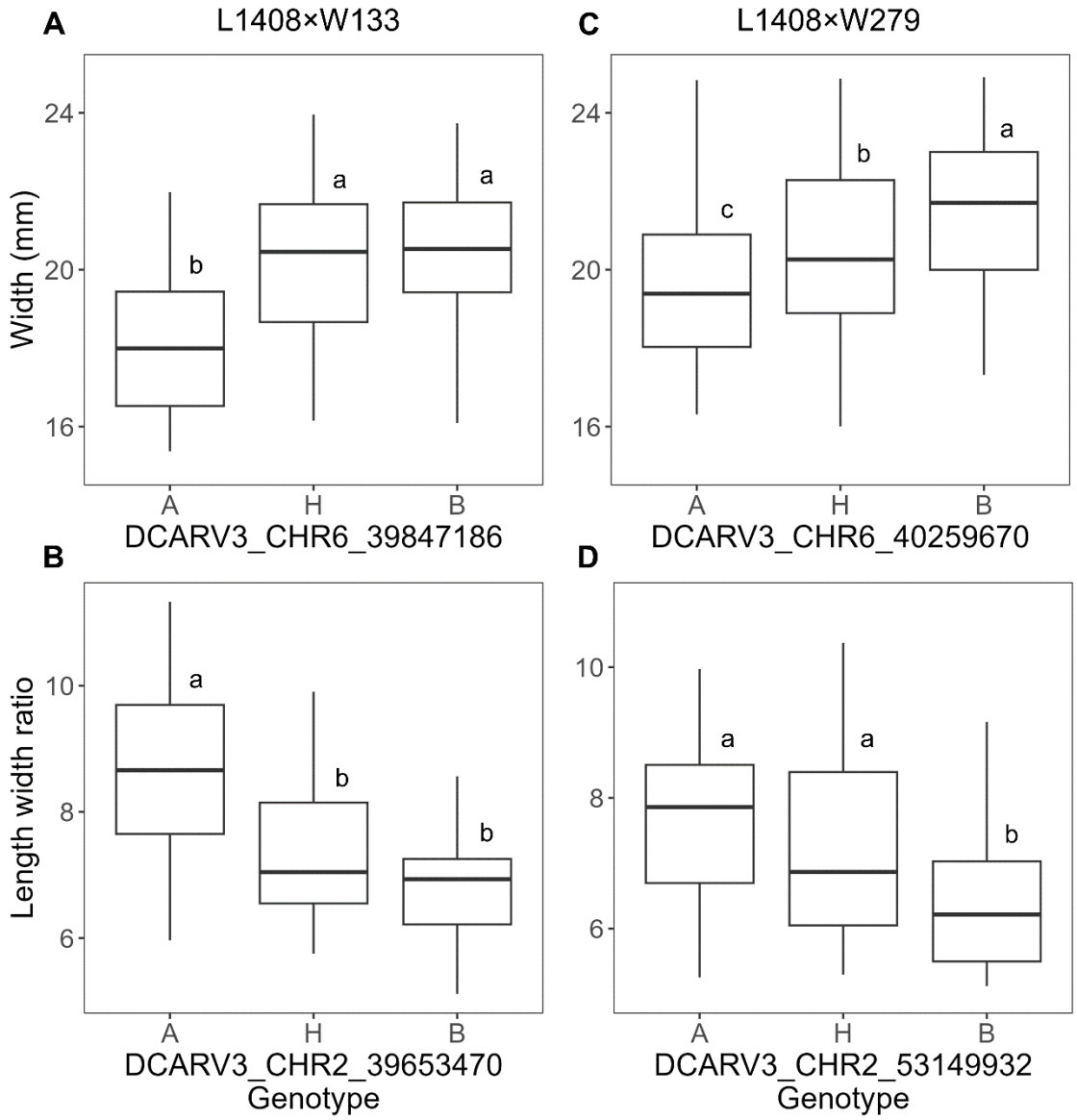

Figure 5
153x156 mm (x DPI)